Electric, thermoelectric and magnetic characterization of γ-Fe2O3 and Co3O4 nanoparticles synthesized by facile thermal...

Article *in* Materials Research Bulletin · November 2017

DOI: 10.1016/j.materresbull.2017.11.002

CITATIONS
0

READS
500

6 authors, including:

E.M.M. Ibrahim
Sohag University
44 PUBLICATIONS **422** CITATIONS
SEE PROFILE

Laila H. Abdel-Rahman
Sohag University
76 PUBLICATIONS **553** CITATIONS
SEE PROFILE

Ahmed M. Abudief
Sohag University
84 PUBLICATIONS **470** CITATIONS
SEE PROFILE

A. M. Ahmed
Sohag University
45 PUBLICATIONS **216** CITATIONS
SEE PROFILE

Materials Research Bulletin 99 (2018) 103–108

Contents lists available at ScienceDirect

Materials Research Bulletin

journal homepage: www.elsevier.com/locate/matresbu

Electric, thermoelectric and magnetic characterization of γ-Fe_2O_3 and Co_3O_4 nanoparticles synthesized by facile thermal decomposition of metal-Schiff base complexes

E.M.M. Ibrahim[a,*], Laila H. Abdel-Rahman[b], Ahmed M. Abu-Dief[b], A. Elshafaie[a], Samar Kamel Hamdan[b], A.M. Ahmed[a]

[a] Physics Department, Faculty of Science, Sohag University, Sohag 82524, Egypt
[b] Chemistry Department, Faculty of Science, Sohag University, Sohag 82524, Egypt

ARTICLE INFO

Keywords:
Fe_2O_3
Co_3O_4
Spinel
Magnetic
Electric

ABSTRACT

Using novel compounds for synthesis of metal oxide nanomaterials can tune their physical properties due to the associated variation in the shape, size and crystallinity. In this work, γ-Fe_2O_3 and Co_3O_4 nanoparticles were successfully prepared by a facile thermal decomposition route, employing $[Fe(C_{32}H_{22}N_4O_2)]\cdot 2H_2O$ and $[Co(C_{16}H_{11}N_3O_4)].^1/_2H_2O$ complexes, respectively as new precursors. The x-ray diffraction and high resolution transmission electron microscopy investigation confirmed that the materials consist of highly pure spinel γ-Fe_2O_3 and Co_3O_4 nanoparticles with average size of ~ 9 and 30 nm, respectively. The electrical conduction is governed by the hopping mechanism. The thermoelectric power measurements confirmed that Co_3O_4 nanoparticles are non-degenerate semiconductor with Fermi energy ~1.21 eV while γ-Fe_2O_3 nanoparticles showed a degenerate to non-degenerate transition. The Co_3O_4 nanoparticles showed a weak ferromagnetic ordering that could be attributed to uncompensated surface spins due to finite-size effects. But γ- Fe_2O_3 NPs show superparamagnetic behavior at room temperature.

1. Introduction

Spinel-type cobalt and iron oxides are known as a promising functional material due to their excellent properties and potential applications. Now, they have been extensively involved in many applications such as heterogeneous catalysts, electrode materials, high density magnetic recording media, printing ink, ferrofluids, pigments, adsorbents, magnetic resonance lithium rechargeable batteries, imaging and gas sensors because they possess outstanding characteristics such as non-toxicity, high resistance to corrosion, durability and low cost [1–7].

Fe_2O_3 and Co_3O_4 nanoparticles (NPs) have been synthesized by many methods. For example, Gage et al. [8] developed magnetically recoverable catalysts via the functionalization of monodisperse iron oxide NPs with commercially available functional linolenic, linoleic and 6-(1-piperidinyl) pyridine-3-carboxlic acids. The synthesized functional materials showed easy magnetic recovery catalyzation and stable catalytic performance which make them promising for commercial use. Kabachi et al. [9] developed novel nanohybrids based on positively charged iron oxide NPs. To provide positive charges, hydrophobic iron oxide NPs were functionalized using specially designed random copolymer of hydrophilic N-methylated DMAEM and hydrophobic SMA units. The NPs are promising for removing the dangerous pollutant from wastewater and producing hydrogen from water using solar energy. Mahmoud et al. [10] synthesized γ-Fe_2O_3 nanocubes through microwave assisted solvothermal technique by using 2,3-oxidosqualene as capping agent for hyperthermia applications. Yuzik-Klimova et al. [11] synthesized flower-like multicore iron oxide crystals in the presence of second and third generation polyphenylenepyridyl dendrons and third generation polyphenylenepyridyl dendrimers as capping molecules. The results demonstrate that the dendron/dendrimer structures and their concentrations control the iron oxide NP size, morphology and the tendency to aggregation.

Although γ-Fe_2O_3 and Co_3O_4 nanoparticles have been synthesized by many methods [1–7,11], there are still several challenges in the synthetic route such as the tendency of γ-Fe_2O_3 and Co_3O_4 to grow into larger or irregular particles. To overcome these challenges and control the growth, organic capping agents are used [11,12]. Using organic capping agents is not environment friendly and increases the cost beside the problem of the phase purity control of the final product. In contrast, thermal decomposition of compounds (particularly the

* Corresponding author.
E-mail address: e.ibrahim@science.sohag.edu.eg (E.M.M. Ibrahim).

http://dx.doi.org/10.1016/j.materresbull.2017.11.002
Received 19 June 2017; Received in revised form 30 October 2017; Accepted 1 November 2017

organometallic molecular precursors) can be regarded as one of the most convenient techniques because it is not only provides good control over purity, composition, homogeneity, phase and microstructure of the resultant products but enables us to avoid complicated synthesis procedures and conditions as well as special instruments [13–19]. Easterday et al. synthesized iron oxide NPs by thermal decomposition of iron oleate in octadecane, eicosane, or docosane as solvents [13,14]. Their works aim to fabricate magnetically recoverable catalysts based on mixtures of Pd/Fe oxide and Ru/Fe oxide NPs for hydrogenation of alkyne alcohols and nitrobenzene. The solvent type, reaction temperature, and the size and composition of initial iron oxide NPs were demonstrated to be the control factors determining synthesis outcomes including the degree of NPs aggregation and catalytic properties.

Although the electrical conduction of γ-Fe_2O_3 and Co_3O_4 has been studied extensively over the last decades to predict and control their performance in the electronic devices, there is a lack of understanding of two main issues. To be specific, there is still significant disagreement on the electrical conduction mechanism and the distribution of the various charge states of Fe and Co in the spinel crystal lattice. Furthermore, as the size of the particles reduces into nanometric scale both oxides exhibit changes in their properties which need further study and investigations. Commonly, it is accepted that Co_3O_4 and γ-Fe_2O_3 are p- and n-type spinel semiconductors, respectively. However, there is consensus of opinion on whether the conduction is intrinsic or due to defects and on how mobile the holes or electrons are [20–25]. Several works suggest that the conduction in the γ-Fe_2O_3 and Co_3O_4 is governed by the small polaron hopping [21,25,26]. However, it has been reported also that charge carriers hopping between the trivalent and divalent cations located in the octahedral and tetrahedral sites of the spinel structure is responsible for the conduction [21,22,25]. Herein, we report a cost-efficient and simple strategy to fabricate γ-Fe_2O_3 (9 nm) and Co_3O_4 (30 nm) NPs via thermal decomposition of [Fe($C_{32}H_{22}N_4O_2$)]· $2H_2O$ and [Co($C_{16}H_{11}N_3O_4$)].1/$2H_2O$, respectively. The study describes an experimental approach to developing our understanding of the electrical transport as well as the magnetic properties of the synthesized γ-Fe_2O_3 and Co_3O_4 NPs. Discussion of some interesting and relevant aspects of the NPs such as conductivity, carriers mobility, type of carriers and magnetic phases is also involved.

2. Experimental

2.1. Materials

All chemicals and solvents such as organic compounds 5-bromosalicyaldehyde (98%) and 2-aminopyridine (97%) were of reagent grade and used as purchased without purification. Ethanol (97%) and acetic acid products were used without distillation. Ferrous ammonium sulphate $(NH_4)_2Fe(SO_4)_2$. $6H_2O$ (98%) and cobalt(II) nitrate hexahydrate $Co(NO_3)_2{\cdot}6H_2O$ (97.95%) were obtained from Sigma −Aldrich.

2.2. Synthesis of Schiff base ligand $C_{16}H_{12}N_2O$

The typical Schiff base ligand was synthesized by the condensation of equimolar ratio of 5-bromosalicyaldehyde (5 mmol, 1.00 g) with 2-aminopyridine (5 mmol, 0.47 g) in 20 ml ethanol. The resulting reaction mixture was refluxed for 1 h at 70C°. After that, the solution was gradually evaporated to quarter of its original volume and then left to cool. The obtained crystals were filtered and then washed with ethanol for several times and dried under reduced pressure in a desiccator.

2.3. Synthesis of Fe (II) and Co (II)Schiff base complexes

Fe (II) Schiff base complex ([Fe($C_{32}H_{22}N_6O_2$)]. $2H_2O$) was synthesized by mixing 20 ml ethanolic solution of the prepared Schiff base ligand (6 mmol, 1.49 g) with 10 ml of aqueous ethanolic solution $(NH_4)_2{\cdot}Fe(SO_4)_2{\cdot}6H_2O$ (3 mmol, 1.18 g). The Co (II) Schiff base complex ([Co($C_{16}H_{11}N_3O_4$)]1/$2H_2O$) was synthesized by adding 15 ml of aqueous ethanolic solution of $Co(NO_3)_2{\cdot}6H_2O$ (5 mmol, 1.46 g) to 15 ml of ethanolic solution of the prepared Schiff base ligand (5 mmol, 1.24 g). In both cases, few drops of glacial acetic acid were added to avoid the oxidation of Fe(II) and Co(II) and the mixture solutions were stirred magnetically for 3 h under nitrogen at 25C°. The resulting solutions were stirred magnetically for 3 h. The obtained products were evaporated overnight. The formed solid products were filtered, washed with ethanol, and then dried in vacuo over anhydrous $CaCl_2$.

2.4. Synthesis of iron and cobalt oxide nanoparticles

The prepared Fe (II) and Co(II) Schiff base complexes were used as precursors for preparing the γ-Fe_2O_3 and Co_3O_4 NPs. The γ-Fe_2O_3 and Co_3O_4 NPs were synthesized by placing 1 g of Fe (II) and Co(II) complexes, respectively into a crucible and heating at 500 °C with heating rate 10 °C/min in air for 1.5 h. The final products were washed with ethanol for at least three times and dried at room temperature, to remove any impurities. By this fast and simple method, metal oxide NPs can be produced without expensive and toxic solvents or complicated equipment.

2.5. Characterization of the prepared cobalt and iron oxides nanoparticles

High resolution transmission electron microscope (HRTEM) studies were performed using a JEOL JEM-2100F transmission electron microscope operated at an accelerating voltage of 200 kV. The samples for HRTEM were dispersed in ethanol, sonicated and sprayed on a carbon-coated copper grid and then allowed to air-dry. The structure of the sample was investigated by the x-ray diffraction (XRD) technique, being the x-ray patterns from 5° to 80° at 2θ with a step of 0.05° and a counting time of 2.5 s/step collected by a Philips X'Pert PRO MPD (PANalytical) using graphite-monochromatized Cu-K_α radiation (λ = 1.54184 Å) operating at 45 kV and 40 mA. The electrical properties were studied by measuring the electrical conductivity as a function of temperature using a so-called two-probe method in the temperature range 300–593 K. The temperature dependence of Seebeck coefficient was determined in order to study the thermoelectric properties of the samples. The measurements were carried out within a temperature range 83–323 K using specially made sample holder. The electrical conductivity and Seebeck coefficient measurements were carried out in a vacuum of 10^{-3} mmHg which was found to contribute much to the thermal stability during the measurements. The temperature of the sample and the temperature gradient in the thermoelectric measurement were sensed by standard copper-constantan thermocouples.

3. Results and discussion

Fig. 1 shows the XRD patterns of the Fe and Co oxide NPs. All the diffraction peaks are corresponding to typical cubic spinel structure of γ-Fe_2O_3 (with lattice parameters a = 8.363 Å in JCPDS card file No. 39–1346) and cubic spinel structure of Co_3O_4 (with lattice parameters a = 8.085 Å, Z = 8 with space group Fd–3 m in JCPDS card file No. 78–1970 phases) [25].

The sharpness of most peaks confirms the good crystallinity of the product. No indications of other Fe and Co based phases were detected. The relatively large broadness of the diffraction peaks indicates the small size of the NPs.

Fig. 2 shows the HRTEM images of the Co_3O_4 and γ-Fe_2O_3 samples. The images imply that the samples consist of agglomerated NPs which can be attributed to the mutual magnetic interaction. The morphology of the NPs were highlighted by HRTEM images at higher magnifications depicted as insets in Fig. 2 (a) and (c) for γ −Fe_2O_3 and Co_3O_4, respectively. The inset of Fig. 2a illustrates that γ −Fe_2O_3 sample consists

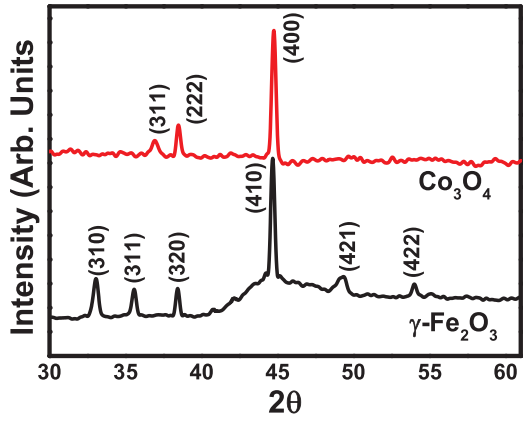

Fig. 1. XRD patterns for γ-Fe2O3 and Co3O4 NPs.

of deformed and poorly crystalline hexagonal platy-like shaped NPs. The inset of Fig. 2(c) shows that Co_3O_4 sample consists of nearly spherical NPs. Fig. 2(b) displays clear lattice fringes in HRTEM image respective to Co_3O_4 NPs with *d* spacing of 0.62 nm coinciding with the cubic spinel cobalt oxide structure and confirming the highly crystalline character of the NPs [22].

The HRTEM investigations allowed to extract and analyze the size and size distribution of the NPs. The results of this analysis are illustrated in Fig. 2(d, e). The size distribution of γ-Fe_2O_3 ranges from 3 to 19 nm, with an average value D_{TEM} 9 ± 0.5 nm (see Fig. 2(c)). The respective histogram for Co_3O_4 (Fig. 2(d)) implies a larger size distribution ranging from 15 to 55 nm with average size amounts to D_{TEM} = 30 ± 1 nm.

Fig. 3a shows the temperature (T) dependence of the electrical conductivity (σ) of the metal oxides at hand. The data reveal that the NPs have low electrical conductivity in order of $10^{-10}\,\Omega^{-1}.m^{-1}$. The low conductivity magnitudes of γ-Fe_2O_3 and Co_3O_4 were reported in other previously published literature [22,27]. For example, the earliest work published by Morin et al. on polycrystalline Fe_2O_3 described very low electrical conductivities in order of $10^{-14}\,\Omega^{-1}.cm^{-1}$ [27]. Also Ibrahim et al. reported a room temperature conductivity value of $\sim 30 \times 10^{-10}\,\Omega^{-1}.cm^{-1}$ for Co_3O_4 NPs synthesized using co-precipitation method [22]. These small values of the electrical conductivity can be explained by Fe^{3+}/Fe^{2+} and Co^{2+}/Co^{3+} valence alternation on spatially localized 3d orbitals. The behavior of σ-T plots depicted in Fig. 3a suggest that electrical conduction in the samples is thermally activated where the conductivity values decrease significantly as the temperature of measurement increases. Several models were suggested to describe the conduction mechanisms in the metal oxides. According to the solid-state theory of semiconductors [23,24], the conduction in a semiconductor with one or more impurity levels, can be described by the following formula:

$$\sigma = \sigma_0 \exp\left(-\frac{E_g}{2kT}\right) + \sum_{i=1}^{n} \sigma'_{0,i} exp\left(-\frac{\Delta E_{ai}}{kT}\right) \quad (1)$$

where, σ_o and $\sigma'_{0,i}$ are constants, E_g is the energy gap (the energy required to transfer the charge carriers from the valence band to the conduction band), E_{ai} is the activation energy (the energy required to transfer the charge carriers between the impurity level number *i* and the conduction band) and *k* is the Boltzmann constant. The first term in Eq. (1) represents the band–band intrinsic conduction mechanism while the second term represents the extrinsic conduction mechanism in the semiconductor. The *Ln(σ)* vs. *1/T* plots (not presented here) of the metal oxides under study show liner behavior in one straight line with one slope indicating that the conduction is represented by one of the above mentioned mechanisms. But, the activation energies were calculated to be *0.09 and 0.1* eV for γ-Fe_2O_3 and Co_3O_4, respectively.

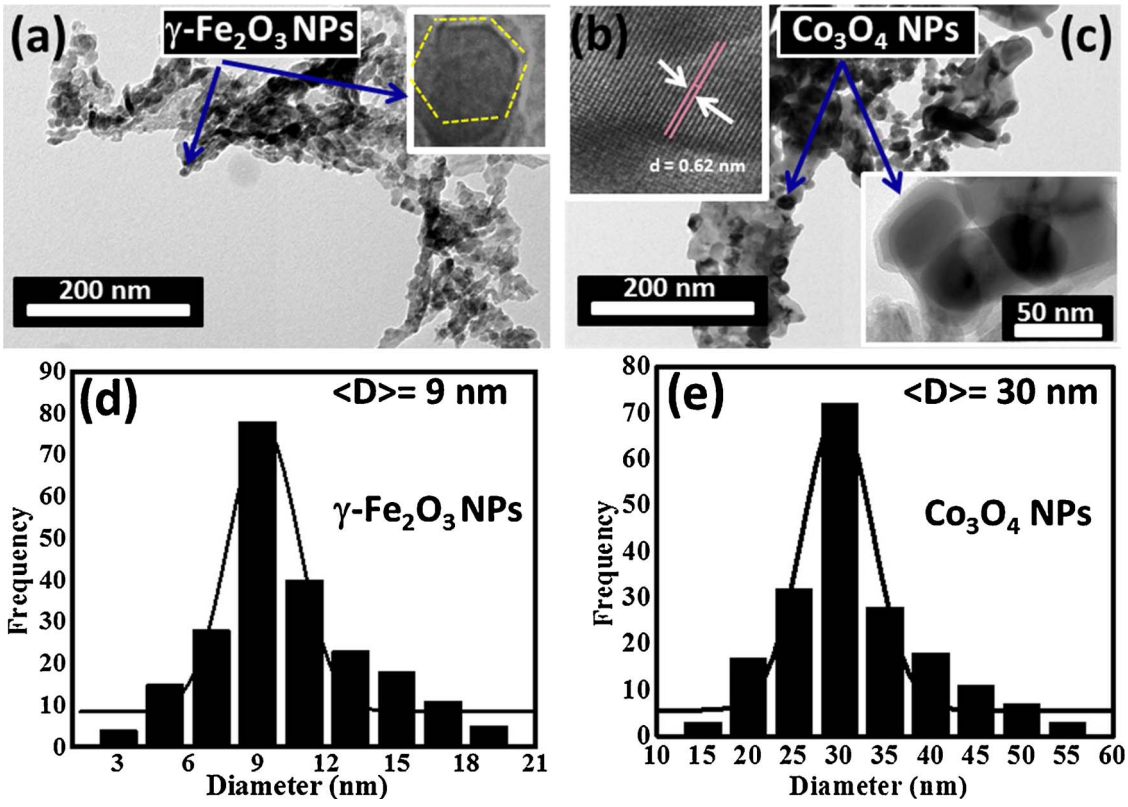

Fig. 2. (a, c) HRTEM images of γ-Fe2O3 and Co3O4 NPs, respectively; (b) HRTEM image shows lattice fringes of Co3O4 NPs; (d, e) Histograms represent the size distribution of γ-Fe2O3 and Co3O4 NPs, respectively; The insets of Figs. (a, b) show HPTEM images at higher magnification highlighting the morphology of γ-Fe2O3 and Co3O4 NPs, respectively at higher magnifications.

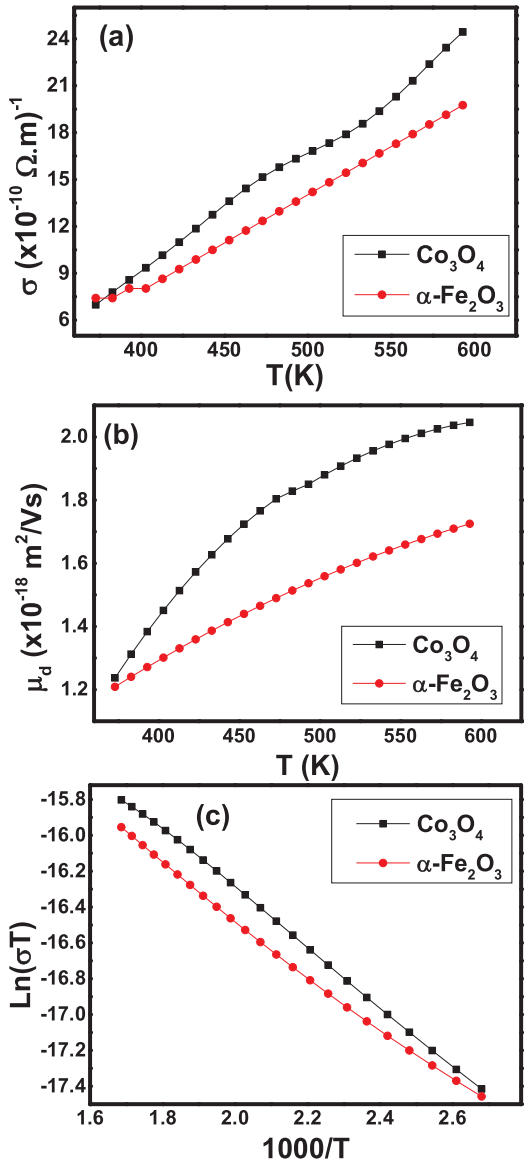

Fig. 3. a) σ vs. T b) μ_d vs. T and c) Ln(σT) vs.1000/T of Co3O4 and γ-Fe2O3 NPs.

These values are much lower than *1* eV indicating that the conduction in the samples is not caused by the transfer of the charge carriers from the filled valence band to the empty conduction band i.e. the intrinsic conduction has omitted in case of our samples [6,25] and only the impurity (extrinsic) conduction may predominate. On the other side, the drift mobility μ_d was calculated using the

formula: $\mu_d = \sigma/ne$ where e is the electron charge and n is the charge carrier concentration given by the formula [28–30].

$$n = 2\left(\frac{2\pi m^* K_B T}{h^2}\right)^{\frac{3}{2}} e^{\left(-\frac{Ea}{K_B T}\right)} \quad (2)$$

where m^* is the effective mass of the charge carrier (assumed to be the rest mass of electron), E_a is activation energy of the conduction process (calculated from Eq. (1)), taking into consideration that this expression is valid when the value of $E_a \geq 3k_BT$ [31,32]. The μ_d −T plots depicted in Fig. 3b show that the drift mobility of our NPs is temperature dependent and have very small values (in order of $10^{-18}\,m^2v^{-1}s^{-1}$) compared to those representing the intrinsic or extrinsic conduction mechanisms ($\sim 10^{-4}-10^{-6}\,m^2v^{-1}s^{-1}$) [27,33]. This means that the conduction in the NPs is not of intrinsic or extrinsic type. Indeed, many modeling studies confirm that the conduction in metal oxides is governed by the mechanism of charge carriers hopping. In particular, in γ-Fe_2O_3 and Co_3O_4 compounds, the charge carriers hopping occurs among the octahedral B-sites. TO be specific, the transition of $Fe^{2+} \leftrightarrow Fe^{3+}$ ions in γ-Fe_2O_3 or $Co^{2+} \leftrightarrow Co^{3+}$ ions in Co_3O_4 might be responsible for the conduction due to hopping of charge carriers between adjacent octahedral B sites [34]. Noteworthy, the conduction behavior, in such case, is determined according whether the charge carriers hopping occurs between the cations (c–c) or the cations/anions (c–a–c) at B sites. If c–c (i.e Fe–Fe or Co-Co) interaction dominates, the conduction becomes metallic while in case of c–a–c (i.e Fe–O–Fe or Co–O–Co) it becomes semiconducting [34]. Clearly, in our samples the interactions Fe–O–Fe in γ-Fe_2O_3 and Co–O–Co in Co_3O_4 are predominant. In case of hopping mechanism, the electrical conductivity is related to the temperature by the following formula [35]:

$$\sigma = \left(\frac{const.}{T}\right) e^{-E_A/K_B T} \quad (3)$$

Note that, E_A involves the total energy required to transfer the charge carriers between the adjacent octahedral B sites. This means it involves the hopping energy (E_{hop}) and the part of energy consumed for the carrier mobility [36]. The values of E_A were calculated from the *Ln(σT)* vs. *1000/T* plots illustrated in Fig. 3c and amount to 0.13 and 0.142 eV for γ-Fe_2O_3 and Co_3O_4, respectively. The data reveal that E_A is slightly higher than the activation energies E_a determined by Eq. (1). If E_a is considered as the mobility activation energies, then the energy consumed in hopping of the charge carriers can be evaluated from the equations: $E_{hop} = E_A - E_a$ to be 0.04 and 0.042 eV for γ-Fe_2O_3 and Co_3O_4, respectively.

The temperature dependence of Seebeck coefficient (S) was measured for the Fe and Co oxide NPs in the temperature range 83K < T < 313 K. The plots depicted in Fig. 4 show the modulus value of Seebeck coefficient ($|S|$) as a function of temperature (T). Remarkably, in case of γ-Fe_2O_3, Seebeck coefficient slightly increases and then decreases after 200 K showing a transition from degenerate to non-degenerate semiconductor behavior, while Co_3O_4 NPs show non-degenerate behavior over the whole temperature of measurement. For degenerate semiconductor and assuming that the material is a quasi-free electron system, the diffusion contribution to thermopower can be described from the formula [37].

$$S = \frac{\pi^2 k_B^2 T}{3eE_f} \quad (4)$$

The E_f value of γ-Fe_2O_3 within temperature range 83 ≥ T ≥ 200 K (the range of degenerate state) was found to be equal to 0.025 eV which is comparable to the thermal energy ($2k_BT$) at room temperature confirming the degeneracy features of the γ-Fe_2O_3 NPs. In the other side, for the non-degenerate part (at T ≥ 200 K), the $|S|$-T plot was well represented by the following formula [38].

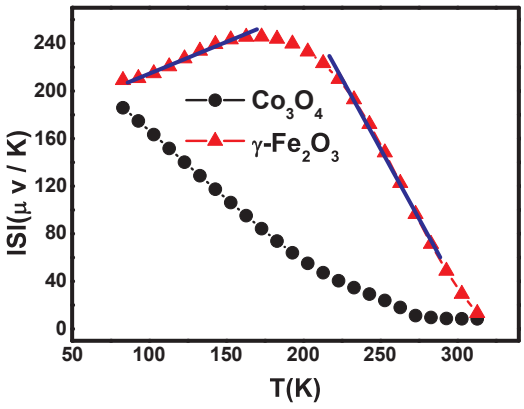

Fig. 4. $|S|$ vs. T of γ-Fe2O3 and Co3O4 NPs.

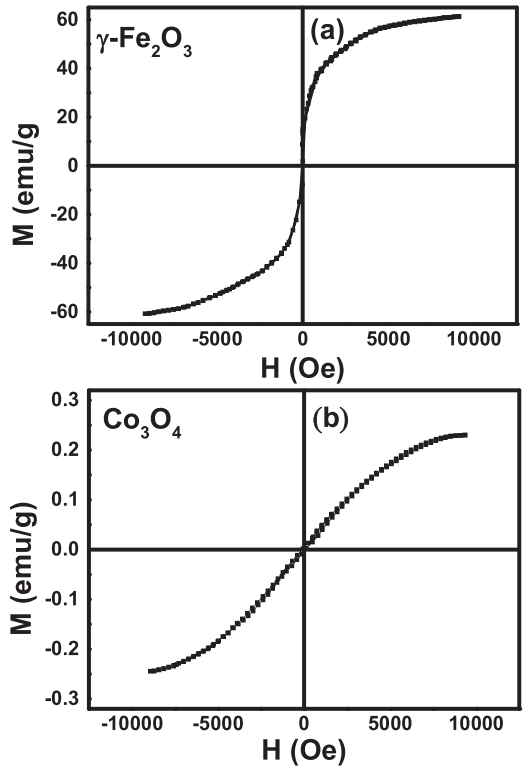

Fig. 5. M vs. H hysteresis loops for a) γ-Fe2O3and b) Co3O4 NPs.

$$S_d = \frac{k_B}{e}\left[\frac{E_f}{k_B T} + \left(r + \frac{5}{2}\right)\right] \quad (5)$$

where E_f is the Fermi energy, k_B is the Boltzmann constant, e is the electron charge and r is scattering parameter. The E_f and r values of the non-degeneracy of γ-Fe_2O_3 was determined to be ~1.70 eV and 1.6, respectively. The obtained magnitudes of E_F is much larger than the thermal energy $2k_BT$ confirming the non-degenerate nature of the sample [39]. Similarly, the $|S|$-T plot of Co_3O_4 can be described by Eq. (5) and the estimated E_f and r values equal to ~1.21 eV and 2.43, respectively.

Magnetic hysteresis measurements were carried out for Co_3O_4 and γ-Fe_2O_3 NPs at room temperature in an applied magnetic field (H) sweeping between ± 10 K Oe. The corresponding magnetization versus magnetic field loops are depicted in Fig. 5. The saturation magnetization M_s value of γ-Fe_2O_3 NPs was estimated from the magnetization M versus H loop (Fig. 5a) to be 60 emu/g, which is lower than the value of bulk maghemite (74 emu/g). Close M_s value was reported by Abbas et al. [40] for chain-like γ-Fe_2O_3 NPs synthesized using chemical method. The reason for obtaining lower magnetization value can be ascribed to the relatively low crystallinity structure of the NPs, as was observed from the HRTEM images. This is reasonable because the low crystallinity of the particles results in formation of magnetic structures with surface spin canting of magnetic moments [41,42]. However, the M_s value of our particles is much higher than those reported for γ-Fe_2O_3 NPs synthesized by other methods. For example, Ali et al. [43] reported M_s ~ 50 emu/g for γ-Fe_2O_3 NPs synthesized using wet chemical method.

The M vs. H loop shows a particularly small hysteresis with a low coercivity (H_c = 30 Oe) for γ-Fe_2O_3 NPs indicating a superparamagnetic behavior. In bulk γ-Fe_2O_3, where the particle size exceeds the domain size, moments reversal is related to the domain wall motion. Reducing of the grain size increases the grain boundaries which in turn act as pinning centers for the domain wall that impede their motion and thus further energy is needed for continuity of the domain wall motion. Therefore, reducing the grain size is expected to create more pinning centers and increases the H_c. However, below a certain critical size (D_{cr}), coherent magnetization reversal of a single magnetic domain is feasible. Quantitatively, D_{cr} amounts to 20–30 nm for γ-Fe_2O_3 [44]. This means that for particles with size smaller than D_{cr}, the coercive field H_c will decrease rapidly as the particle size decreases ($H_{c\alpha}D^6$) [45] and the material exhibit non-hysteretic feature or superparamagnetic behavior.

The room temperature M vs. H loop depicted in Fig. 5b indicates that the Co_3O_4 NPs have weak ferromagnetic ordering in contrary to bulk Co_3O_4 which is typical antiferromagnetic system. The antiferromagnetic systems should have zero magnetic moment per particle due to complete compensation of the sub-lattice spins. As the material size goes down to nanoscale, the case of our Co_3O_4 NPs, the weak ferromagnetic features can be attributed mainly to the breaking of a large number of exchange bonds of the surface atoms which induces an uncompensated magnetic moments in the NPs [17,22]. The values of the remanent magnetization (M_r) and coercivity (H_c) were extracted to be M_r = 0.04 emu/g and H_c = 96 Oe. The weak ferromagnetic ordering was also reported for Co_3O_4 NPs (size of 30–50 nm) by Salavati-Niasari et al. [11] with H_c = 700.7 Oe and M_r = 9.05 emu/g. However, Gopinath et al. reported H_c = 49.32 Oe and M_r = 9.2 emu/g for Co_3O_4 NPs of size ~22 nm.

Fig. 6 shows the temperature (T) dependence of the AC magnetic susceptibility (χ) for the materials at hand. The χ vs. T plot of the Co_3O_4 NPs reveal that χ increases with the increase of temperature up to a certain value T_N and then decreases in a typical antiferromagnetic-paramagnetic transition. The Néel temperature T_N were determined from the Curie-Weiss plot by extrapolating the inverse of susceptibility lines to intersect with the temperature axis to be 123 K. The T_N values were found to be much higher than the reported values of the bulk Co_3O_4 (40 K). Therefore, it is a possibility that the determine transition temperature is a measurement of blocking temperature rather than the Néel temperature due to the ferromagnetic ordering exhibited by the Co_3O_4 NPs as was shown from the hysteresis loop measured in Fig. 5 [46]. This is consistent with Mørup et al. [46,47] who reported that the magnetic structure of the tiny particles is often similar to that of the bulk material, but there are several examples of the effect of the size on the magnetic structures. For γ-Fe_2O_3 NPs, χ increases with the increase of temperature up to T = 163 K and then decreases due to the reduction in magnetic spin disorder induced by thermal energy. For tiny particle magnetic systems, the surface anisotropy plays a significant role in the magnetic behavior. It controls the spin orientation with respect to the normal direction at the surface or at the interface of the magnetic structure. It depends on the particle diameter through $D^{-\alpha}$, where D is the particle diameter and α is close to unity [48,49]. That makes the NPs with large surface area to volume ratio possess a high anisotropy constant. Due to the magnetic anisotropy and also the mutual interaction between the γ-Fe_2O_3 NPs below the blocking temperature

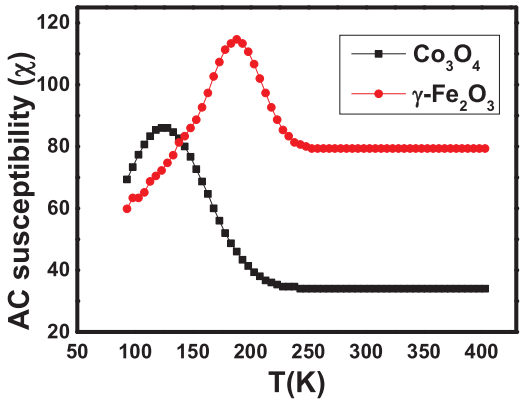

Fig. 6. AC. Magnetic susceptibility vs. temperature for γ-Fe2O3 and Co3O4 NPs.

T_B = 163 K, χ suddenly drops showing superparamagnetic to ferromagnetic transition [50–52].

The experimental value of the blocking temperature allow to determine a rough estimation of the average nanoparticle size using the formula $KV = 25k_BT_B$ [53], where K is the anisotropy constant (=0.4 9 104 J/m3 for bulk γ-Fe_2O_3), V is the nanoparticle volume and k_B is the Boltzmann constant. Under the assumption that the NPs have uniform spherical shape, the calculation gives values 27 nm. The value of the later is higher than average particle size determined from the HRTEM investigation which can possibly be attributed to that the shape of most NPs is not perfectly spherical.

4. Conclusion

In conclusion, γ-Fe_2O_3 and Co_3O_4 NPs were successfully prepared by thermal decomposition of [Fe $(C_{32}H_{22}N_4O_2)$]·$2H_2O$ and [Co $(C_{16}H_{11}N_3O_4)$].½H_2O complexes, respectively as new precursors. The XRD and HRTEM studies revealed the formation of spinel-type γ-Fe_2O_3 and Co_3O_4 with average particle size about 9 and 30 nm, respectively. The electrical measurements confirm that the intrinsic and extrinsic conduction mechanisms are omitted in the synthesized samples due to the low activation energy and low carriers mobility, but the electrical conduction is governed by the hopping mechanism. The thermoelectric measurements showed that the γ-Fe_2O_3 NPs exhibit degenerate to nondegenerate transition while Co_3O_4 NPs have degenerate behavior over the whole temperature range of measurements. The γ-Fe_2O_3 NPs show typical superparamagnetic behavior at room temperature while Co_3O_4 NPs show weak ferromagnetic ordering at room temperature due to the size confinement effect.

References

[1] M. Feygenson, A. Kou, L.E. Kreno, A.L. Tiano, J.M. Patete, F. Zhang, M.S. Kim, V. Solovyov, S.S. Wong, M.C. Aronson, Phys. Rev. B 81 (2010) 014420.
[2] L.H. Abdel-Rahman, R.M. El-Khatib, L.A.E. Nassr, Ahmed M. Abu-Dief, Fakhr El-Din. Lashin, Spectrochim. Acta Part A 111 (2013) 266–276.
[3] A.K. Singh, M.A. Quraishi, Int. J. Electrochem. Sci 7 (2012) 3222–3241.
[4] K. Karthik, G.K. Selvan, M. Kanagaraj, S. Arumugam, N.V. Jaya, J. Alloys Compd. 509 (2011) 181–184.
[5] S.A. Saleh, S.M. Khalil, E.M.M. Ibrahim, Supercond. Sci. Technol. 20 (2012) 372.
[6] Marin Tadic, Dobrica Nikolic, Matjaz Panjan, Graeme R. Blake, J. Alloys Compd. 647 (2015) 1061–1068.
[7] Mahnaz Ghiasi, Azim Malekzadeh, Hamidreza Mardani, Mater. Sci. Semicond. Process. 42 (2016) 311–318.
[8] Samuel H. Gage, Barry D. Stein, Linda Zh. Nikoshvili, Valentina G. Matveeva, Mikhail G. Sulman, Esther M. Sulman, David Gene Morgan, Ekaterina Yu. Yuzik-Klimova, Waleed E. Mahmoud, Lyudmila M. Bronstein, Langmuir 29 (2013) 466–473.
[9] Yurii A. Kabachi, Alexandre S. Golub, Sergey Yu Kocheb, Natalia D. Lenenko, Sergey S. Abramchuk, Mikhail Yu Antipin, Pyotr M. Valetsky, Barry D. Stein, Waleed E. Mahmoud, Ahmed A. Al-Ghamdi, Lyudmila M. Bronstein, Chem. Mater. 25 (2013) 2434–2440.
[10] Waleed E. Mahmoud, Faten Al-Hazmi, Fowzia Al-Noaiser, A.A. Al-Ghamdi, Lyudmila M. Bronstein, Superlattices Microstruct. 68 (2014) 1–5.
[11] E.Yu. Yuzik-Klimova, N.V. Kuchkina, S.A. Sorokina, D.G. Morgan, B. Boris, L. Zh. Nikoshvili, N.A. Lyubimova, V.G. Matveeva, E.M. Sulman, B.D. Stein, et al., Magnetically recoverable catalysts based on polyphenylenepyridyl dendrons and dendrimers, RSC Adv. 4 (44) (2014) 23271–23280.
[12] Y. Dong, K. He, L. Yin, A. Zhang, Nanotechnology 18 (2007) 435602.
[13] Rosemary Easterday, Clara Leonard, Olivia Sanchez-Felix, Yaroslav B. Losovyj, Maren Pink, Barry D. Stein, David Gene Morgan, Nadezhda A. Lyubimova, Linda Zh Nikoshvili, M. Esther Sulman, Waleed E. Mahmoud, Ahmed A. Al-Ghamdi, Lyudmila M. Bronstein, ACS Appl. Mater. Interfaces 6 (2014) 21652–21660.
[14] R. Easterday, O. Sanchez-Felix, Y. Losovyj, M. Pink, B.D. Stein, D.G. Morgan, M. Rakitin, V. Yu. Doluda, M.G. Sulman, W.E. Mahmoud, A.A. Al-Ghamdid, Lyudmila M. Bronstein, Catal. Sci. Technol. 5 (2015) 1902–1910.
[15] E.M.M. Ibrahim, Silke Hampel, Raghunandan Kamsanipally, Juergen Thomas, Kati Erdmann, Susanne Fuessel, Christine Taeschner, Vyacheslav O. Khavrus, Thomas Gemming, Albrecht Leonhardt, Bernd Buechner, Carbon 63 (2013) 358–366.
[16] Tony Jaumann, E.M.M. Ibrahim, Silke Hampel, Diana Maier, Albrecht Leonhardt, Bernd Büchner, Chem. Vap. Deposition 17 (2013) 1–7.
[17] E.M.M. Ibrahim, Silke Hampel, A.U.B. Wolter, M. Kath, A.A. El-Gendy, R. Klingeler, Christine Täschner, Vyacheslav O. Khavrus, Thomas Gemming, Albrecht Leonhardt, Bernd Büchner, J. Phys. Chem. C 116 (2012) 22509.
[18] E.M.M. Ibrahim, Silke Hampel, Jürgen Thomas, Diana Haase, A.U.B. Wolter, Vyacheslav O. Khavrus, Christine Täschner, Albrecht Leonhardt, Bernd Büchner, J. Nanopart. Res. 14 (2012) 1118.
[19] Vyacheslav O. Khavrus, E.M.M. Ibrahim, Alicja Bachmatiuk, Mark H. Rümmeli, A.U.B. Wolter, Silke Hampel, Albrecht Leonhardt, J. Nanopart. Res. 14 (2012) 914.
[20] T. Sugimoto, S. Waki, H. Itoh, A. Muramatsu, J. Colloids Surfaces A 109 (1996) 155–165.
[21] H. Liang-shu, L. Jin-song, C. Han-pu, S. An-min, W. Wei-guo, W. Li-jun, J. Adv Mater. 18 (2006) 2426–2431.
[22] E.M.M. Ibrahim, Ahmed M. Abu-Dief, A. Elshafaie, A.M. Ahmed, Mater. Chem. Phys. 192 (2017) 41–47.
[23] Q.-J. Sun, X.-G. Lu, G.-Y. Liang, Mater. Lett. 64 (2010) 2006–2008.
[24] A.P. Mishra, R.K. Jain, J. Chem. Pharm. Res. 2 (2010) 51–61.
[25] X. Wang, X. Chen, L. Gao, H. Zheng, Z. Zheng, Y. Qian, J. Phys. Chem. B 108 (2004) 16401–16404.
[26] Wei Wang, Jane Y. Howe, Baohua Gu, J. Phys. Chem. C 112 (2008) 9203–9208.
[27] K. Sivula, Photoelectrochemical Hydrogen Production, Chapter 4, Electronic Materials: Science & Technology 102, DOI 10.1007/978-1-4614-1380-6_4, Springer Science + Business Media, LLC 2012.
[28] F.J. Morin, J.P. Maita, Phys. Rev 96 (1954) 28.
[29] E.H. Puutley, W.H. Mitchell, Proc. Phys. Soc. 72 (1958) 193.
[30] A. Martin, Green J. Appl. Phys. 67 (1990) 15.
[31] Y. Aydogdu, F. Yakuphanoglu, A. Aydogdu, M. Sekerci, C. Alkan, I. Aksoy, Mater. Lett. 54 (2002) 352–358.
[32] M.G.A.E. Wahed, K.A. El Manakhly, A. Amer, J. Mater. Sci. Lett. 15 (1996) 919–921.
[33] E.M.M. Ibrahim, Appl. Phys. A 89 (2007) 203–208.
[34] D. Vanidha, A. Arunkumar, S. Rajagopan, R. Kannan, J. Supercond Nov. Magn. 26 (2013) 173–182.
[35] N.F. Mott, E.A. Davis, Electronic Process in Non-crystalline Materials, Clarendon Press, UK, 1979.
[36] N.F. Mott, J. Non-Cryst. Solids 1 (1969) 1.
[37] H.J. Trodahl, Phys. Rev. B 51 (1995) 6175.
[38] G.S. Nolas, J. Sharp, H.J. Goldsmid, Thermoelectrics—Basic Principles and New Materials Developments, Springer Press Germany, 2001, pp. 36–42.
[39] K.X. Zhang, X.Y. Qin, H.X. Xin, H.J. Li, J. Zhang, J. Alloys Compd. 484 (2009) 498–504.
[40] Mohamed Abbas, Md. Nazrul Islam, B. Parvatheeswara Rao, M.O. Abdel-Hamed, Cheol Gi Kim, J. Ind. Eng. Chem. 31 (2015) 43–46.
[41] A.G. Roca, D. Niznansky, V.J. Poltierova, B. Bittova, G.M.A. Ferná ndez, C.J. Serna, M.P. Morale, J. Appl. Phys. 105 (2009) 114309.
[42] M. Abbas, M. Takahashi, C. Kim, J. Nanopart. Res. 15 (2013) 1354.
[43] Kashif Ali, A.K. Sarfraz, Imran M. Mirza, A. Bahadur, S. Iqbal, A. ul Haq, Curr. Appl. Phys. 15 (2015) 925–929.
[44] G. Bate, E.P. Wohlfarth (Ed.), Ferromagnetic Materials, 2 Elsevier, North Holland, 1980, p. 439.
[45] S.A. Majetich, J.H. Scott, E.M. Kirkpatrick, K. Chowdary, K. Gallagher, M.E. McHenry, Nanostruct. Mater. 9 (1997) 291–300.
[46] S. Mørup, D.E. Madsen, C. Frandsen, C.R.H. Bahl, M.F. Hansen, J. Phys.: Condens. Matter 19 (2007) 213202.
[47] J.C. Debnath, Jianli Wang, R. Zeng, J. Magn. Magn. Mater. 421 (2017) 422–427.
[48] D.A. Dimitrov, G.M. Wysin, Phys. Rev. B 50 (1994) 3077–3084.
[49 D.A. Dimitrov, G.M. Wysin, Phys. Rev. B 51 (1995) 11947–11950.
[50] C. Pereira, A.M. Pereira, P. Quaresm, P.B. Tavares, E. Pereira, J.P. Araújo, C. Freire, Dalton Trans. 39 (2010) 2842–2854.
[51] Y. Huang, J. Lin, Y. Bando, C. Tang, C.Y. Zhi, Y.G. Shi, E. Takayama-Muromachibc, D. Golberg, J. Mater. Chem. 20 (2010) 1007–1011.
[52] E.M.M. Ibrahim, J. Appl. Phys. 113 (2013) 154301.
[53] V.B. Barbeta, R.F. Jardim, P.K. Kiyohara, F.B. Effenberger, L.M. Rossi, J. Appl. Phys. 107 (2010) 073913.